OPEN ACCESS
Journal of Mechanics in Medicine and Biology
(2023) 2350075 (12 pages)

DOI: 10.1142/S0219519423500756

COMPARING THE MESOSCALE AND MICROSCALE MECHANICAL PROPERTIES OF RAT LUNG TISSUE USING COMPUTATIONAL MODELING

ELIZABETH DIMBATH*, STEPHANIE GEORGE†,
LISANDRA DE CASTRO BRÁS‡ and ALEX VADATI†,§

*Department of Biomedical Engineering, Pratt School of Engineering
Duke University, Durham, NC, USA

†Department of Engineering, College of Engineering and Technology
East Carolina University, Greenville NC, USA

‡Department of Physiology, Brody School of Medicine
East Carolina University, Greenville, NC, USA
§vahdatia18@ecu.edu

Received 9 April 2023
Accepted 13 June 2023
Published 4 August 2023

Current literature reports a wide range of stiffness values and constitutive models for lung tissue across different spatial scales. Comparing the reported lung tissue stiffness values across different spatial scales may provide insights into how well those mechanical properties and the proposed constitutive models represent lung tissue's mechanical behavior. Thus, this study applies *in silico* modeling to compare and potentially bridge the differences reported in lung tissue mechanical properties at different length scales. Specifically, we predicted the mesoscale mechanical behavior of rat lung tissue based on *in situ* and *in vitro* microscale test data using finite element (FE) analysis and compared those computational predictions to the reported data using mesoscale uniaxial experiments. Our simulations showed that microscale-based stiffness values differed from the mesoscale data in the simulated strain range of 0–60%, with the atomic force microscopy (AFM)-based data overestimating the mesoscale data above 15% strain. This research demonstrates that computational modeling can be used as an informative and guiding tool to investigate and potentially bridge the differences in reported lung tissue material properties across length scales.

Keywords: Lung mechanics; mechanical behavior; multiscale mechanics; lung parenchyma; mechanical testing; computational modeling.

§Corresponding author.

1. Introduction

The function of the lung in terms of gas transport and exchange depends on the lung tissue's mechanical properties. Pathologies of the respiratory system such as acute respiratory distress syndrome (ARDS) pneumonia, pulmonary fibrosis, and emphysema can lead to changes in the mechanics of the respiratory zone, hence reducing gas exchange capability.[1] Therefore, as abnormalities affecting lung mechanics are found in many lung diseases, it is essential to understand the mechanical properties of lung tissue.[2] The complex structure of the lung gives rise to different manifested mechanical properties at various spatial scales. The organ scale emergent mechanical properties arise from the hierarchical lung structure and properties of the extracellular matrix (ECM) components, predominantly collagen and elastin.[2] The fiber network within the ECM is the tissue's primary stress-bearing component and aids in controlling the expansion and contraction of alveoli, therefore protecting the gas exchange regions from damage.[3] However, at the mesoscale, parenchyma is composed mainly of the air-filled acini, small airways, respiratory bronchioles, and alveolar ducts. Figure 1 outlines the structure of the lung from the alveolar septa up to the whole lung level.

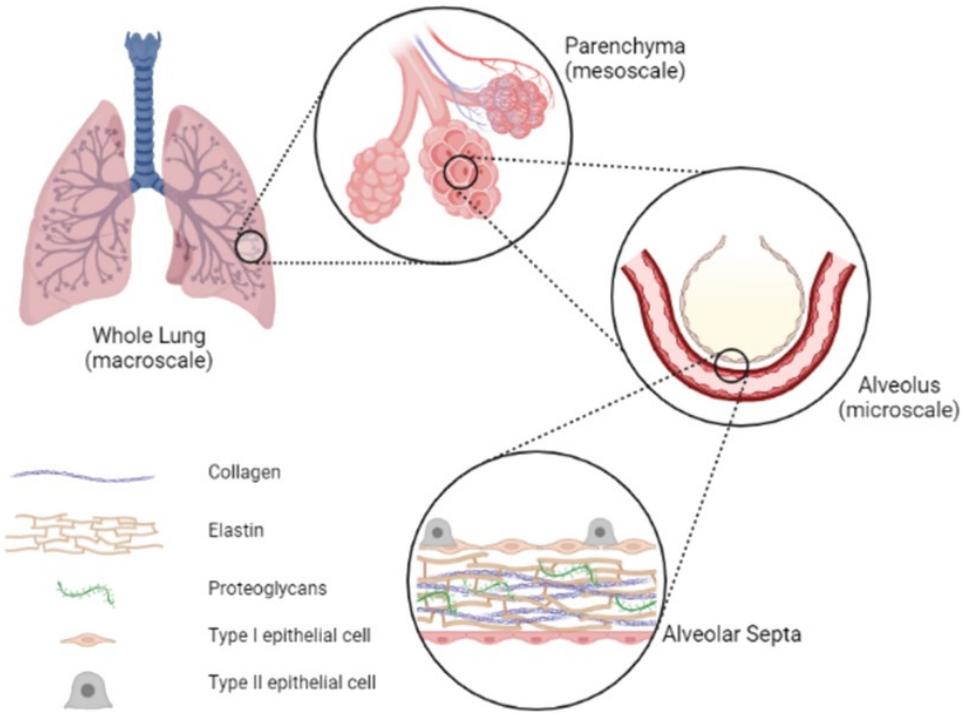

Fig. 1. The hierarchical structure of the lung across spatial scales. The ECM components of the alveolar septa bring about the emergent mechanical properties of the lung at the mesoscale and organ scale. (created in BioRender.com by the first author)

Computational models can provide a noninvasive and potentially subject-specific approach to understanding the mechanics of breathing and the effects of heterogeneous disease on lung function.[4] The geometry, spatial scale, and mechanical properties assigned to *in silico* models are essential components of credible computational models that produce accurate results. Some of the first models that laid the foundation for the computational modeling of alveolar mechanics were developed by Mead *et al.*[5] and Dale *et al.*[6] More recent models have largely expanded upon those early models to study mechanics of both the healthy and disease states of the lung tissue at the microscale, including models that studied a single alveolus,[6,7] or an alveolar sac.[8,9] Additionally, the idealized 3D truncated octahedral geometry has been shown to be capable of simulating parenchymal tissue mechanics by reasonably estimating the alveolar geometry and with lower computational cost compared to microCT-based models.[7,10]

Even though mechanical testing studies of lung parenchyma have offered valuable insight into tissue properties, a wide range of moduli have been reported for lung tissue at the mesoscale. Rausch *et al.*[11] and Birzle *et al.*[12] demonstrated the discrepancies between several constitutive models developed for parenchymal tissues. Hence, careful consideration must be given to using accurate mesoscale mechanical properties of the lung in computational models. Furthermore, there is disagreement on the reported mechanical properties of lung tissue at the microscale. With the use of atomic force microscopy (AFM),[13–15] among other techniques, there have been discrepancies in the reported stiffness values of lung tissue, partially due to different experimental setups, specimen size, and testing protocols. In addition, some approaches only accounted for the linear behavior of lung tissues, reporting a single Young's modulus to characterize the stiffness.[13,15]

Consequently, comparing and potentially reconciling the reported stiffness values of lung tissue across spatial scales may provide insights into how well those values represent lung tissue behavior. As the emergent mesoscale mechanical properties of the parenchyma are dependent on the microscale properties of the alveolar septa, reported values at the microscale must be accurate before they can be used in meso- and macroscale lung models. Hence, this study aims to use *in silico* modeling to compare the differences reported in lung tissue mechanics at different length scales. Specifically, the objective of this research is to utilize computational modeling for the purpose of studying whether the emergent mechanical properties of lung tissue at the mesoscale, based on two microscale mechanical testing data sets, are consistent with the experimental data reported at the mesoscale. Therefore, we aimed to predict the mesoscale mechanical behavior of rat lung tissue using finite element (FE) and subsequently compared those predictions to mesoscale experimental results.

2. Methods

Using FE analysis, the mesoscale mechanical behavior of lung tissue strips was predicted based on previously reported *in vitro* and *in situ* microscale experiments.

Mechanical properties at the microscale were taken from the results reported by two different research groups that determined the mechanical behavior of rat lung tissue using distinct approaches (described in Sec. 2.2).[15,16] The emergent properties from the FE model were then compared to mesoscale data from a study that utilized a coupled approach to determine the mechanical behavior of rat parenchyma.[12] The strategy and stages of the study are summarized in Fig. 2. Further details on the methods of our study are given below.

2.1. *Model geometry*

The 3D geometry of the model comprised of an array of alveoli is represented by truncated octahedra.[17] The geometry modeled the tissue slices used in the uniaxial tension testing of Birzle *et al.*[12] SolidWorks 2022 (Dassault Systems, France) was used to build the geometry where each truncated alveolus was assigned the average dimensions of a rat alveolus.[18,19] The entire structure had overall height, width, and depth dimensions equal to the average dimensions of lung tissue slices used for uniaxial tension testing in Birzle *et al.*,[12] with the length, width, and thickness set to 2.2, 7, and 1.1 mm, respectively (Fig. 3). The geometry was imported into COMSOL Multiphysics v6.1 for FE analysis (COMSOL Multiphysics, MA, USA). Each constitutive model from the two microscale studies, described in the next subsection, was applied to the walls of the truncated octahedra.

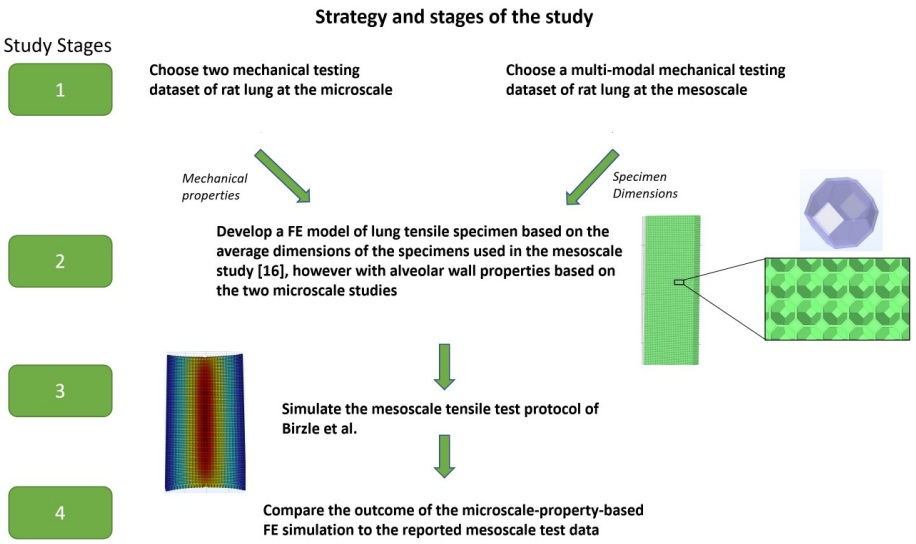

Fig. 2. A flowchart demonstrating the strategy for and the stages of this study. We chose a high-fidelity mechanical testing dataset at the microscale[16] and two data sets at the mesoscale.[14,16] Then, we developed a FE model of a lung tissue strip with the overall height, width, and depth corresponding to the specimens used by Birzle *et al.*[12,20] for uniaxial tensile testing. The FE model was based on a truncated octahedron model of an alveolus with the alveolar wall mechanical properties assigned according to microscale mechanical testing datasets.

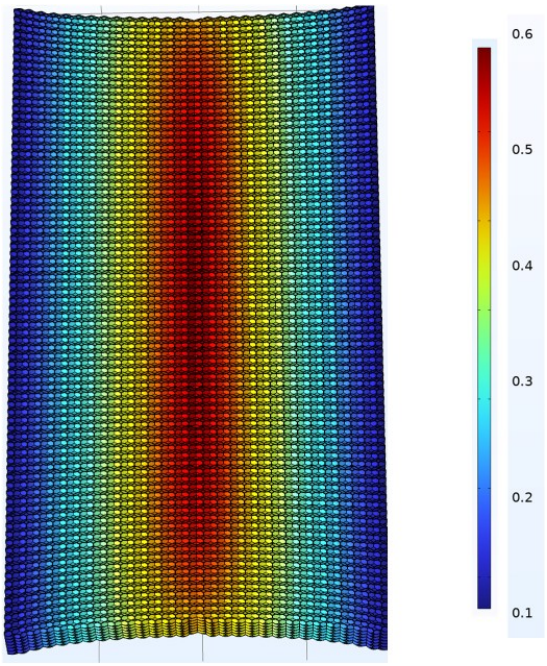

Fig. 3. Representative result of uniaxial tension testing of 3D FE model at maximum displacement. The microscale constitutive models were applied to the walls of the truncated octahedra, then uniaxial tension testing was simulated to measure the resulting reaction force.

2.2. *Constitutive models*

In this study, three microscale material models were used in the FE model, and the emergent mesoscale behavior was compared to the mesoscale model of Birzle *et al.*,[20] which utilized a coupled experimental approach to account for the isochoric and volumetric behavior of lung parenchyma. Birzle *et al.*'s mesoscale study proposed a hyperelastic constitutive model[20] with the strain energy density function defined as follows:

$$\varphi = 356\,\mathrm{Pa}(I_1 - 3) + 331.7\,\mathrm{Pa}(I_3^{-1.075} - 1) + 197.4\,\mathrm{Pa}(I_3^{-\frac{1}{3}} I_1 - 3)^3 + 5.766\,\mathrm{Pa}(I_3^{\frac{1}{3}} - 1)^6, \quad (1)$$

where I_1 and I_3 are the first and third invariants of the right Cauchy–Green deformation tensor, respectively. Additionally, the viscoelastic behavior of the specimen was accounted for using the rheological standard linear solid (SLS) model as described by Birzle *et al.*[20]

We simulated the mesoscale specimen of Birzle *et al.*[12] by implementing Eq. (1) in Comsol Multiphysics and simulating a block of tissue in a tensile test. Subsequently, the mesoscale results based on Ref. 12 were used as a baseline for comparing the

emergent properties resulting from simulations carried out using the microscale-based models for the assemblage of alveoli.

To develop the micro-scale-based model using the assemblage of alveoli, the nonlinear microscale materials models of Perlman and Wu[16] and Jorba *et al.*[14] were applied to the septa walls. In the microscale study by Perlman and Wu,[16] a novel technique quantified the behavior of the alveolar septa *in situ* to account for the change in moduli across pressure ranges. Since the study included both the tissue elastic forces and interfacial forces, surface tension's effects were first removed from the constitutive model before using it in our FE analysis. Equation (2), as defined by Perlman and Wu,[16] determined the tissue-only behavior:

$$E_{\text{tissue}} = E_{\text{effective}} - 2\left(T_H - \frac{T_L}{[\bar{t}(\bar{e}_H - \bar{e}_L)]}\right), \tag{2}$$

where T, $\bar{t}$ and $\bar{e}$ correspond to the surface tension, septal thickness, and strain over a specified pressure range, with subscripts H and L corresponding to the high and low pressure values, respectively. Once the effect of surface tension were removed from the material model of Perlman and Wu,[16] the resulting stress and strain values were fit to a Yeoh hyperelastic material model using HYPERFIT (www.hyperfit.wz.cz), a calibration software that uses stress–strain data to determine constants for a given constitutive model. The Yeoh model's strain energy density function is given by:

$$W = \sum_{i=1}^{3} C_i (I_1 - 3)^i + \sum_{i=1}^{3} \frac{1}{D_i} (J-1)^{2i}, \tag{3}$$

where, C_i and D_i are material constants that characterize the isochoric and volumetric elastic response of the tissue, respectively, I_1 is the invariant of the right Cauchy–Green deformation tensor and J is the elastic volume ratio for which the isochoric invariant of the right Cauchy–Green deformation tensor is defined as $\bar{I}_1 = J^{-2/3} I_1$.

Finally, to capture the material's time-dependent behavior, the SLS viscoelastic model, based on the work of Birzle *et al.*,[20] was added to the Yeoh constitutive model. The evolution equation of the viscoelastic stress (σ_q) of the SLS model was described by the equation:

$$\frac{1}{\tau}\sigma_q + \dot{\sigma_q} = \beta \dot{\sigma}^{\infty}, \tag{4}$$

where τ is a relaxation time, β is the nondimensional free energy factor, and σ^{∞} is the equilibrium second Piola–Kirchhoff stress tensor. β was assigned the value of 0.8525 and τ was set to 0.09936 s.[20]

The second microscale material model applied to the alveolar septa was the Yeoh hyperelastic model of Jorbal *et al.*[14] based on their AFM experiments using spherical tips. Again, the SLS model of viscoelasticity was added to the hyperelastic model to ensure all simulations were performed at the same loading rate. All material properties used in the study are summarized in Table 1.

Table 1. The three microscale-based constitutive models used in 3D FE analysis which were compared to the compressible mesoscale model of Birzle *et al.*[12]

Study	Length scale	Constitutive model	Parameters
Birzle *et al.*	Mesoscale	Visco-hyperelastic	Hyperelastic model's coefficients given in Eq. (1); $\beta = 0.8525$ and $\tau = 0.09936\,\text{s}$
Perlman & Wu (without surface tension effects)*	Microscale	Visco**-Hyperelastic (Yeoh*)	$C_1 = 0.71\,\text{kPa}$, $C_2 = 8.1\text{e-}10\,\text{kPa}$, $C_3 = 3.7\,\text{kPa}$, $D_1 = 0.01\,\text{kPa}^{-1}$, $D_2 = 0\,\text{kPa}^{-1}$, $D_3 = 0\,\text{kPa}^{-1}$; $\beta = 0.8525$, $\tau = 0.09936\,\text{s}$
Jorba *et al.* Spherical tip	Microscale	Visco**-Hyperelastic (Yeoh)	$C_1 = 1.3\,\text{kPa}$, $C_2 = 8.9\,\text{kPa}$, $C_3 = 26.2\,\text{kPa}$, $D_1 = 0.009\,\text{kPa}^{-1}$, $D_2 = 0\,\text{kPa}^{-1}$, $D_3 = 0\,\text{kPa}^{-1}$; $\beta = 0.8525$, $\tau = 0.09936\,\text{s}$

Notes: *Model calibrated using HYPERFIT software
**The viscoelastic effects were added to hyperelastic model based on the results of Ref. 23.

2.3. *Boundary conditions and simulation settings*

Uniaxial tension tests were simulated by pulling on one end of the geometry while keeping the opposing end fixed (clamped), similar to the experiments of Birzle *et al.*[20] A fixed displacement, corresponding to the change in length reported by Birzle *et al.*[12] was used to reach the desired strain, and the resulting reaction force was measured. Symmetry conditions were applied to the geometry to decrease the computational cost of the simulations. The first Piola–Kirchhoff stress and engineering strain were calculated and plotted for each specimen. Finally, the emergent properties from the computational model were compared to the mesoscale study of Birzle *et al.*[12]

The geometry was meshed with 4,400,000 reduced integration quadratic tetrahedral elements. The simulations were run on a workstation with dual Intel Xeon Gold 20-Core CPUs, using Comsol's Nonlinear Structural Mechanics package. A time-dependent solver with the implicit Backward Differentiation Formula (BDF) time-stepping scheme, and the Parallel Direct Sparse Solver (PARDISO) were used. A mesh convergence study was performed by varying the mesh density until the change in stress output was less than 0.5%.

3. Results

Figure 3 shows the FE model under uniaxial tension at the maximum displacement. The resulting stress–strain curves are shown in Fig. 4. Across the tested strain range of the virtual experiments, the results from Jorba *et al.*'s[14] AFM-based study overestimated the mesoscale stiffness with a normalized root mean square error (NRMSE) value of 4.59. However, the simulation results based on the *in situ*

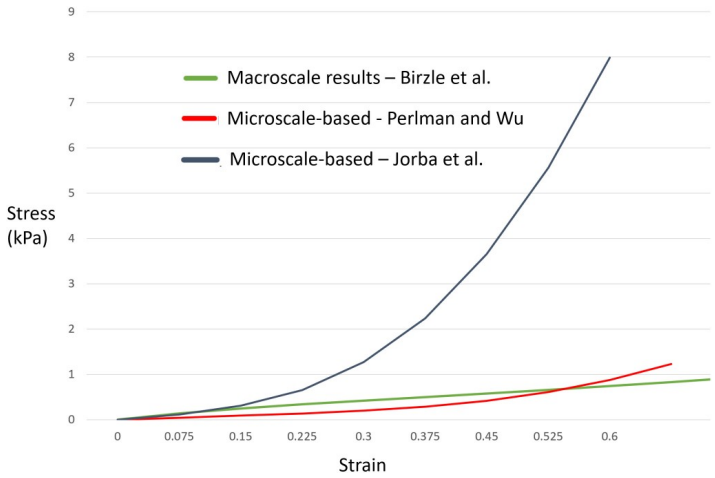

Fig. 4. Stress–strain curve comparing the emergent properties from microscale[14,16] to data at mesoscale[20] across the strain range simulated. Across the whole strain range, the microscale model based on the work of Jorba *et al.*[14] overestimated the reported mesoscale values, whereas at strains below 52%, the microscale visco-hyperelastic model based on the work of Perlman and Wu[16] underestimated the reported mesoscale data.

experiments of Perlman and Wu showed a smaller difference from the mesoscale results of Birzle *et al.* with an NRMSE of 1.14 (Fig. 4). Specifically, the simulated curve based on the work of Perlman and Wu[16] underestimated the mesoscale data below 52% strain. Above 52% strain, the model based on Perlman and Wu's[16] data overestimated the mesoscale data of Birzle *et al.*[12,20]

4. Discussion

Since many studies evaluating lung tissue mechanical properties at the micro and mesoscales have reported a wide range of moduli for lung tissue, it is essential to carefully consider the experimental setup, in addition to the spatial and temporal scales of the mechanical tests, to obtain relevant and accurate values of stiffness for use in computational modeling. In this study, we utilized computational modeling to compare the emergent mechanical properties of lung tissue at the mesoscale based on microscale mechanical testing data. We chose three of the most comprehensive mechanical testing datasets published by other researchers for the purpose of this study: The microscale *in situ* data reported by Perlman and Wu,[16] the microscale AFM-based data of Jorbal *et al.*,[14] and the mesoscale data of Birzle *et al.*[12] Overall, this comparative study showed that the microscale and mesoscale lung mechanical testing data reported by different groups exhibit large differences. However, the data reported by Perlman and Wu[14,16] showed a smaller difference to the mesoscale data of Birzle *et al.*[20] compared to the AFM-based data of Jorba *et al.*[14] (Fig. 4). Furthermore, this study showed that FE modeling could be used as an informative and

guiding tool to investigate and compare differences in reported lung tissue mechanical properties across length scales.

It has been suggested that tidal breathing generates relatively low strains in the septal wall of the lung alveoli.[21] Within the range of physiological tidal breathing, studies in mammalian lungs estimate that the alveolar tissue undergoes only about 4–10% strain[22] and up to 20% strain in exercise.[23] However, when inflated from functional residual volume to total lung capacity, the alveolar strain can increase to anywhere between 15–40% in a heterogeneous manner throughout the lung volume.[21,24] Therefore, strains below 40% are of greater interest when comparing emergent properties of microscale lung, particularly in the healthy state. The AFM-based model of Jorba *et al.*[14] showed a close agreement with the mesoscale measurements of Birzle *et al.*[12] up to 15% strain after which the two models considerably diverged from each other. On the other hand, the constitutive model based on Perlman and Wu's[16] work exhibited an overall smaller difference to the mesoscale when the full strain range of up to 60% was considered (Fig. 4). Of note, strains greater than 40% may not be relevant in the healthy lung but may become more crucial in disease states where heterogeneous damage can lead to greater strains in injured areas of the lung.[21] As computer models gain importance in such circumstances, it becomes more important that constitutive models defining lung's mechanical behavior are accurate across scales and wide strain ranges.

At the microscale, Perlman and Wu[16] determined an effective modulus to capture the effects of elastic and interfacial forces in the alveolar septum during inflation while at the mesoscale, Birzle *et al.*[12] aimed to couple uniaxial tension testing with volume–pressure change experiments to describe the isochoric and volumetric nonlinear behavior of lung parenchyma. Both studies utilized novel approaches to characterize the material behavior of the lung at different length scales that employed the effects of inflation on tissue behavior.[12,16] The microscale AFM-based study of Jorba *et al.*[21] was also novel in terms of its experimental setup but appears to overestimate the tissue stiffness considerably at strains above 15% compared to the mesoscale data of Birzle *et al.*[12]

Moreover, considering that mechanical test data from multiple studies was analyzed here, the comparison carried out in this study required caution to ensure comparisons were made reasonably. For instance, the study by Perlman and Wu[16] included surfactant and thus incorporated effects of different alveolar components. To nullify this effect, a mathematical equation was used to determine the tissue-only behavior (Eq. (2)). It is important to note that the constitutive models utilized in this study do not explicitly model the behavior of the individual tissue constituents, such as the collagen and elastin fibers, but rather model the combined behavior. Several factors may have contributed to the differences seen between the reported mesoscale data and the emergent properties from microscale models seen in this study. While all studies were based on rat lung tissue, the species of rat differed among the studies and there could also be differences in age of specimens, which can affect lung

mechanics.[13,25] The microscale study of Perlman and Wu[16] utilized male Sprague–Dawley rats while the mesoscale study of Birzle *et al.*[12] tested lung tissue from female Wistar rats. The age of rats used in each study was not reported. Along with the differences in the experimental setup for determination of each constitutive model utilized in this study, there were also assumptions made in the development of the FE model used for comparison. The dimensions of the FE model were based on average dimensions from a range given by Birzle *et al.*[12] Also, all material model parameters were based on the averages reported by other researchers and therefore did not consider the large standard deviations typically associated with animal tissue testing. Moreover, since there is a lack of experimental data on the anisotropic mechanical behavior of lung tissue at the microscale, only isotropic models of tissue behavior were used in this study. Additionally, in our idealized geometry, the truncated octahedra were fully enclosed with no open pathways through alveolar walls for airflow. Removal of some alveolar walls to form the alveolar ducts would provide a more realistic geometry.

In conclusion, this comparative study allowed for comparing of lung tissue mechanical properties across micro and mesoscale. Considering the inherent variation in animal testing data and limitations of the model, Perlman and Wu's[16] was in closer agreement with the mesoscale data of Birzle *et al.*[12] than Jorba *et al.*[14] data. By comparing the emergent properties of simulated microscale-based models to the material behavior reported at the mesoscale, this research sheds new light on the need for reconciling and bridging the lung's mesoscale and macroscale mechanical properties. This study demonstrated that FE modeling can be used as an informative and guiding tool to investigate and potentially resolve differences in reported lung tissue material properties across different spatial scales.

Funding

This material is based on the work supported by the National Science Foundation under award # 2034964. The authors acknowledge Research Computing at The University of Virginia for providing computational resources and technical support that have contributed to the results reported within this publication. URL: https://rc.virginia.edu. The material in this publication is based upon work supported in part by the National Science Foundation under the ACCORD Grant (Award #: 1919667). Any opinions, findings, conclusions or recommendations expressed in this material are those of the author(s) and do not necessarily reflect the views of the National Science Foundation.

Competing Interests

The authors have no relevant financial or nonfinancial interests to disclose.

References

1. Suki B, Bates JHT, Extracellular matrix mechanics in lung parenchymal diseases, *Respir Physiol Neurobiol* **163**(1–3):33–43, 2008, doi: 10.1016/j.resp.2008.03.015.
2. Suki B, Bates JHT, Lung tissue mechanics as an emergent phenomenon, *J Appl Physiol* **110**(4):1111–1118, 2011, doi: 10.1152/japplphysiol.01244.2010.
3. Wilson TA, Bachofen H, A model for mechanical structure of the alveolar duct, *J Appl Physiol Respir Environ Exerc Physiol* **52**(4):1064–1070, 1982.
4. Middleton S *et al.*, Towards a multi-scale computer modeling workflow for simulation of pulmonary ventilation in advanced COVID-19, *Comput Biol Med* **145**:105513, 2022, doi: 10.1016/J.COMPBIOMED.2022.105513.
5. Mead J, Takishima T, Leith D, Stress distribution in lungs: A model of pulmonary elasticity, *J Appl Physiol* **28**(5):596–608, 1970, doi: 10.1152/jappl.1970.28.5.596.
6. Dale PJ, Matthews FL, Schroter RC, Finite element analysis of lung alveolus, *J Biomech* **13**(10):865–873, 1980, doi: 10.1016/0021-9290(80)90174-8.
7. Concha F, Sarabia-Vallejos M, Hurtado DE, Micromechanical model of lung parenchyma hyperelasticity, *J Mech Phys Solids* **112**:126–144, 2018, doi: 10.1016/j.jmps.2017.11.021.
8. Koshiyama K, Nishimoto K, Ii S, Sera T, Wada S, Heterogeneous structure and surface tension effects on mechanical response in pulmonary acinus: A finite element analysis, *Clin Biomech* **66**:32–39, 2019, doi: 10.1016/j.clinbiomech.2018.01.001.
9. Ghasafari P, Bin I, Ibrahim M, Pidaparti R, Strain-induced inflammation in pulmonary alveolar tissue due to mechanical ventilation, *Biomech Model Mechanobiol* **16**(4):1103–1118, 2017, doi: 10.1007/s10237-017-0879-5.
10. Sarabia-Vallejos MA, Zuñiga M, Hurtado DE, The role of three-dimensionality and alveolar pressure in the distribution and amplification of alveolar stresses, *Sci Rep* **9**:8783, 2019, doi: 10.1038/s41598-019-45343-4.
11. Rausch SMK, Martin C, Bornemann PB, Uhlig S, Wall WA, Material model of lung parenchyma based on living precision-cut lung slice testing, *J Mech Behav Biomed Mater* **4**(4):583–592, 2011, doi: 10.1016/j.jmbbm.2011.01.006.
12. Birzle AM, Martin C, Uhlig S, Wall WA, A coupled approach for identification of nonlinear and compressible material models for soft tissue based on different experimental setups — Exemplified and detailed for lung parenchyma, *J Mech Behav Biomed Mater* **94**:126–143, 2019, doi: 10.1016/j.jmbbm.2019.02.019.
13. Sicard D, Haak AJ, Choi KM, Craig AR, Fredenburgh LE, Tschumperlin DJ, Aging and anatomical variations in lung tissue stiffness, *Am J Physiol Lung Cell Mol Physiol* **314**(6):L946–L955, 2018, doi: 10.1152/ajplung.00415.2017.
14. Jorba I *et al.*, Nonlinear elasticity of the lung extracellular microenvironment is regulated by macroscale tissue strain, *Acta Biomater* **92**:265–276, 2019, doi: 10.1016/j.actbio.2019.05.023.
15. Melo E *et al.*, Effects of the decellularization method on the local stiffness of acellular lungs, *Tissue Eng C Meth* **20**(5):412–422, 2014, doi: 10.1089/ten.tec.2013.0325.
16. Perlman CE, Wu Y, In situ determination of alveolar septal strain, stress and effective Young's modulus: An experimental/computational approach, *Am J Physiol Lung Cell Mol Physiol* **307**(4):L302, 2014, doi: 10.1152/ajplung.00106.2014.
17. Denny E, Schroter RC, Viscoelastic behavior of a lung alveolar duct model, *J Biomech Eng* **122**(2):143–151, 2000.
18. Cavalcante FSA *et al.*, Mechanical interactions between collagen and proteoglycans: Implications for the stability of lung tissue, *J Appl Physiol* **98**(2):672–679, 2005, doi: 10.1152/japplphysiol.00619.2004.

19. Mercer RR, Laco JM, Crapo JD, Three-dimensional reconstruction of alveoli in the rat lung for pressure-volume relationships, *J Appl Physiol (1985)* **62**(4):1480–1487, 1987, doi: 10.1152/JAPPL.1987.62.4.1480.
20. Birzle AM, Wall WA, A viscoelastic nonlinear compressible material model of lung parenchyma — Experiments and numerical identification, *J Mech Behav Biomed Mater* **94**:164–175, 2019, doi: 10.1016/j.jmbbm.2019.02.024.
21. Roan E, Waters CM, What do we know about mechanical strain in lung alveoli?, *Am J Physiol-Lung Cell Mol Physiol* **301**(5): L625–L635, 2011, doi: 10.1152/ajplung.00105.2011.
22. Knudsen L, Ochs M, The micromechanics of lung alveoli: Structure and function of surfactant and tissue components, *Histochem Cell Biol* **150**(6):661–676, 2018, doi: 10.1007/s00418-018-1747-9.
23. Fredberg JJ, Kamm RD, Stress transmission in the lung: Pathways from organ to molecule, *Annu Rev Physiol* **68**:507–548, 2006, doi: 10.1146/annurev.physiol.68.072304.114110.
24. Perlman CE, Bhattacharya J, Alveolar expansion imaged by optical sectioning microscopy, *J Appl Physiol* **103**(3):1037–1044, 2007, doi: 10.1152/japplphysiol.00160.2007.
25. Bou Jawde S, Takahashi A, Bates JHT, Suki B, An analytical model for estimating alveolar wall elastic moduli from lung tissue uniaxial stress-strain curves, *Front Physiol* **11**:121, 2020, doi: 10.3389/fphys.2020.00121.